EFFECT OF ECCENTRICITY ON THE STATIC AND DYNAMIC PERFORMANCE OF A TURBULENT HYBRID BEARING*

Luis A. San Andres
Mechanical Engineering Department
Texas A&M University
College Station, Texas 77843-3123, U.S.A.

The effect of journal eccentricity on the static and dynamic performance of a water lubricated, 5-recess hybrid bearing is presented in detail. The hydrostatic bearing has been designed to operate at a high speed and with a large level of external pressurization. The operating conditions determine the flow in the bearing to be highly turbulent and strongly dominated by fluid inertia effects. The analysis covers the spectrum of journal center displacements directed towards the middle of a recess and towards the mid-land portion between 2 consecutive recesses. Predicted dynamic force coefficients are uniform for small to moderate eccentricities. For large journal center displacements, fluid cavitation and recess position determine large changes in the bearing dynamic performance. The effect of fluid inertia force coefficients on the threshold speed of instability and whirl ratio of a single mass flexible rotor is discussed.

INTRODUCTION

Hydrostatic and hybrid(combined hydrostatic and hydrodynamic) journal bearings (HJBs) have recently been the subject of increased attention because of their potential applications as support elements in cryogenic high speed turbomachinery. These bearings have been proposed because of their high radial stiffness, accuracy of positioning and good vibration damping characteristics. Despite these attractive features, the hydrodynamic action at high speeds may bring the potential of half speed whirl instability. Thus, it is of importance to determine the limits of safe operation for such bearing applications

To provide the levels of load support needed in high speed machinery operating with cryogenic fluids requires large external pressure supplies. These unique operating conditions give rise to large film Reynolds numbers, and cause the flow within the bearing film to be highly turbulent and strongly dominated by fluid inertia effects both at the recess edges and in the thin film land regions. Conventional analytical treatments are confined to the numerical solution of the Reynolds equation for turbulent flow, and thus, can not interpret correctly the actual complex phenomena occuring in HJBs.

*The present research effort has been sponsored by Rocketdyne, by the NASA Center for Space Technology, and by the State of Texas Advanced Technology Program.

NOMENCLATURE

b	Recess circumferential length [m].
c	radial clearance [m]
$C_{XX}, C_{XY}, C_{YX}, C_{YY}$	damping coefficients [Ns/m]
C_d	Orifice discharge coefficient
D	2 R . Bearing diameter [m].
d_o	Orifice diameter [m]
F_x, F_y	Fluid film forces in X and Y directions [N].
$f_J = 0.001375 \left[1 + \left(\frac{5x10^5}{R_J}\right)^{1/2.65}\right]$	Turbulent friction factor at journal surface
$f_B = 0.001375 \left[1 + \left(\frac{5x10^5}{R_B}\right)^{1/2.65}\right]$	Turbulent friction factor at bearing surface
h	$H/c = 1+\varepsilon_x\cos\theta + \varepsilon_y\sin\theta$ Dimensionless film thickness.
H_r	Recess depth [m].
I_1, I_2, I_4	Inertia coefficients for stability analysis.
$K_{XX}, K_{XY}, K_{YX}, K_{YY}$	Stiffness coefficients [N/m]
K_{eq}	Equivalent bearing stiffness coefficient [N/m].
K_r	Half of rotor stiffness [N/m].
k_x, k_y	$(1/2)(k_J+k_B)$ dimensionless shear parameters in circumferential and axial directions
k_J, k_B	$f_J R_J$, $f_B R_B$. Turbulent shear parameters at journal and bearing surfaces.
L	Bearing axial width [m].
l	Recess axial length [m].
N_{rec}	Number of recesses on bearing.
$M_{XX}, M_{XY}, M_{YX}, M_{YY}$	Inertia or added mass coefficients [Kg].
M_r	Half of rotor mass [Kg].
P	Fluid pressure [N/m^2].

P_s	External supply pressure [N/m^2].
Qr	$\int H\,(V.n)\,d\Gamma_r$. Recess flow into film lands [m3/s]
Re	$\rho\Omega cR/\mu$ Nominal circumferential flow Reynolds number.
Re_p	$\rho c^3(P_s-P_a)/\mu^2 R$ Pressure flow Reynolds number.
Re_p^*	(Re_p) (c/R) Modified pressure flow Reynolds number.
R_J, R_B	$(\rho/\mu)H[(U-\Omega R)^2+V^2]^{1/2}$, $(\rho/\mu)H[U^2+V^2]^{1/2}$. Reynolds numbers at journal and bearing surfaces.
To	Fluid film resistance torque [Nm]
U,V	mean flow velocities in circumferential and axial dirs.
V_r	$(H_r+H)A_r+V_s$ Total recess volume [m^3] .
V_s	Volume of orifice supply line [m^3].
{X,Y}	Inertial coordinate system.
α_i	relative effective fluid inertia mass at support.
β	Fluid compressibility factor [m^2/N].
ε_x, ε_y	$(e_x,e_y)/c$. Dimensionless journal eccentricities in X & Y directions
Λ	$\mu\Omega R^2/c^2(Ps-Pa)$. Rotational speed parameter.
ϕ	ω_s/Ω_s. Whirl frequency ratio.
ϕ_o	Whirl frequency ratio without fluid inertia effects.
ω	Excitation or whirling frequency [1/sec]
ω_s	Whirl frequency at instability threshold [1/sec].
Ω	Rotational speed of journal [1/s]
Ω_s	Threshold speed of instability [1/s].

Redecliff and Vohr (1969), Heller (1974), and Deguerce et al. (1975) have presented finite difference solutions to the turbulent flow Reynolds equation. Reported numerical flow rates and hydrodynamic forces are lower than experimental measurements but considered satisfactory. Artiles, Walowit, and Shapiro (1982) presented a well documented numerical method for prediction of the static and dynamic performance characteristics of turbulent HJBs. The analysis includes the local effect of fluid inertia at the recess edges, but the fluid compressibility effect at the recess volumes is neglected. The turbulence model employed by Artiles seems to give inconsistant results in the transition

from pressure dominated flow to pure shear flow at high speed operation.

The influence of fluid inertia at the recess edges and hydrodynamic pressure generation within the recess for high rotational speeds have been shown and discussed in detail in the experimental work of Chaomleffel and Nicholas (1986). The magnitude of the measured edge pressure drop appears to be dependent on the journal rotational speed and the recess depth. Comparisons of the experiments with predictions based on a finite difference solution to the turbulent Reynolds equation with fluid inertia effects are also included in the same reference. The numerical calculations for load and flow rate were found to be always greater than the measurements, and predicted edge pressure drops were determined to be smaller than those observed.

SanAndres(1989a) has developed a full inertial numerical analysis for accurate prediction of the performance characteristics of orifice compensated turbulent HJBs. The analysis departs from the mean flow Navier-Stokes equations and includes the effect of recess volume fluid compressibility. The numerical results presented by SanAndres (1989b) indicate that fluid inertia at the film lands acts as an additional flow resistance, and thus, causes reduced flow rates and greater hydrodynamic effects when compared to an inertialess solution. Inertia force coefficients of large magnitude in bearings handling large density fluids and with low values of the clearance ratio (c/R) are reported. The full inertial analysis developed by the author shows a considerable improvement over conventional analyses based on the classical Reynolds equation.

The present paper introduces further numerical predictions for a high speed HJB currently under testing. The effect of journal eccentricity on the static and dynamic performance of the sample bearing are throughly detailed. A simple analysis to determine the influence of fluid inertia on the threshold speed of instability for a simple flexible rotor supported on hybrid bearings is presented.

ANALYSIS

Figure 1 presents the geometry of a hydrostatic journal bearing. Fluid passes across a restrictor orifice and a recess area of relatively large clearance, and then flows through the film lands to the bearing discharge. The performance characteristics of the bearing are governed by momentum and continuity considerations in the fluid film lands as well as flow continuity through the bearing recesses. The former defines the pressure and velocity fields over the bearing lands, whereas the latter provides values for the pressure in the recesses.

San Andres (1989a) presented a derivation of the appropriate equations for fully turbulent flow in hybrid bearings. The analysis considers the effect of fluid inertia (advection and temporal terms) at the film lands and a local Bernoulli type inertia effect at the recess edges. For an isoviscous incompressible fluid, the continuity and momentum equations for the turbulent bulk flow on the film lands are given as

$$\frac{\partial}{\partial x}(UH) + \frac{\partial}{\partial y}(VH) + \frac{\partial H}{\partial t} = 0 \qquad (1)$$

$$-H\frac{\partial P}{\partial x} = \frac{\mu}{H}\left(k_x U - k_J \frac{R\Omega}{2}\right) + \rho\left\{\frac{\partial}{\partial t}(HU) + \frac{\partial}{\partial x}(HU^2) + \frac{\partial}{\partial y}(HUV)\right\} \qquad (2)$$

$$-H\frac{\partial P}{\partial y} = \frac{\mu}{H} k_y V + \rho\left\{\frac{\partial}{\partial t}(HV) + \frac{\partial}{\partial x}(HUV) + \frac{\partial}{\partial y}(HV^2)\right\} \qquad (3)$$

The turbulent shear parameters k_x and k_y are taken as local functions of the friction factors relative to the journal and bearing surfaces (Hirs, 1973, Nelson, 1987).

The continuity equation at the recess is defined by the global balance between the flow through the orifice restrictor, the recess outflow into the film lands, and the temporal change of fluid mass in the recess volume. The recess continuity equation is then given by

$$C_d \frac{\pi d_o^2}{4}\left[\frac{2(P_s - P_r)}{\rho}\right]^{1/2} = Q_r + \frac{\partial V_r}{\partial t} + V_r\,\beta\,\frac{\partial P_r}{\partial t} \qquad (4)$$

where β represents the fluid compressibility factor at the recess volume. The recess outflow into the film lands, Q_r, is determined by integration of the mean flow velocity vector along a closed path Γ_r encompassing the recess boundary.

For hybrid operation a pressure rise occurs within the downstream portion of the recess (Chaomleffel et al.,1985). This region is considered as a one-dimensional step bearing. The local acceleration of fluid from relatively stagnant conditions at the recess to a high velocity at the film lands causes a sudden pressure drop at the recess boundary. The pressure at the entrance to the film lands is modeled by simple Bernoulli type relations based on the theory developed by Constantinescu (1975).

San Andres (1989a) presented a numerical procedure for effective solution of the nonlinear governing equations (1) through (5). The numerical method is based on the SIMPLEC algorithm of Van Doormal & Raithby (1984) for iterative solution of the film land equations, and it is combined with a Newton-Raphson algorithm for estimation of recess pressures and satisfaction of the recess flow constraints. The flow field is divided into a zero-th and first order fields describing the equilibrium condition and perturbed dynamic motion, respectively. Solution of the zero-th order field gives the steady state bearing characteristics such as flow, load and friction torque. The first order field determines the dynamic force coefficients for the excitation frequency of interest.

RESULTS

A Hydrostatic-Hybrid Bearing Test program is under development at Texas A&M University. The purpose of the program is to develop an experimental data base and analytical capabilities for turbulent flow hydrostatic bearings. The objectives of the program are to design and build a test apparatus, systematically test the bearings, and develop an analysis to predict the bearing characteristics and anchor it to the test data.

The hydrostatic bearing test apparatus has been designed and is currently under preliminary testing. Table 1 presents a description of the 5 recess test hydrostatic bearing considered as a test case. The working fluid is hot water at a temperature of 71.1C(160F), and the maximum rated inlet supply fluid pressure is 7.23 MPa(1050 psi). The rotor speed ranges from 0 to 500Hz(30000 rpm), and the bearing and journal surfaces are considered perfectly smooth. For the conditions shown in Table 1, the flow within the bearing is highly turbulent with dominance of hydrodynamic effects at the highest rotational speed. The large value of the modified Reynolds number, Re_p^*, shows that fluid inertia at film lands will have a considerable influence on the test bearing static and dynamic performance characteristics.

The orifices of the test bearing have been sized for a concentric pressure ratio equal to 0.5 at the maximum operating speed of 30000 rpm. This condition implies that the predicted pressure drop between the supply and recess pressures is equal to the pressure drop between the recess and the outside of the bearing. The selected concentric pressure ratio is not necessarily an optimum for the present bearing configuration but was chosen on the grounds of common practice for establishing bearing stiffnesses which are not too far from optimum. For an orifice discharge coefficient equal to one, the present full inertial analysis predicted an orifice diameter equal to 1.496mm.

A complete analysis has been carried out to determine the effects of journal center eccentricity on the static and dynamic performance characteristics of the test bearing at 30000 rpm and an external supply pressure equal to 6.54 Mpa(950psi). The journal center displacements ranged from the concentric position to eccentricity radii equal to 90% of the film clearance in the directions toward the middle of a recess and toward the mid-point in the lands between two consecutive recesses. Figure 2 shows the predicted bearing flow rate and the film friction torque for the range of journal displacements considered. The flow rate is a maximum at the concentric position and decreases as the eccentricity increases. The friction torque is a minimum at the centered position and increases rapidly as the journal center displacement approaches the bearing clearance. The increment in torque and reduction in flow rate are due to increased flow resistance for growing eccentricities. The results show the flow and the torque to appear closely as even functions of the eccentricity. The maximum reduction in flow rate at the largest eccentricity considered, $(e/c)=0.9$, is approximately equal to 22% of the flow at the centered position, while the increment in torque is about 30%.

Figure 3 shows the calculated recess pressures for different values of the static journal eccentricity. Negative eccentricities, ε_x, denote journal displacements to the midland between recesses 1 and 5 located at 36^o and 324^o, respectively. Positive eccentricities, ε_x, denote journal displacements toward the middle of recess 3 located at 180^o. Figure 4 shows the entire pressure field

over the journal surface for selected values of the journal center displacement. At the concentric position the recess pressures are identical and the bearing has null load capacity. The pressure field for null eccentricity is depicted in Figure 4(c).

For displacements toward the middle of a recess, Figure 3 shows that maximum recess pressures are attained at recesses 2 and 3 located in the converging portion of the film thickness. The large pressures attained at the second recess are caused by the effect of journal rotation and will generate a substantial film force normal to the journal displacement. For eccentricity radii larger than 0.5, cavitation was found to appear in the land region around recess 4 where the film thicknesses is diverging. Figures 4(d) and 4(f) show the pressure field for eccentricities ε_x equal to 0.4 and 0.7, respectively; note that for large journal displacements there is a significant hydrodynamic effect between recesses 2 and 3.

For displacements toward the midland between recesses 1 and 5, Figure 3 shows that maximum recess pressures are located at recess 5 in the convergent portion of the film thickness while low recess pressures are attained at recesses 2 and 3 in the divergent film thickness region. Fluid cavitation is predicted to occur for eccentricities larger than 0.6. Figures 4(a) and 4(b) show the pressure field for eccentricities ε_x equal to -0.7 and -0.4, respectively. Note from Figure 3 that for large journal displacements toward the land between the recesses, the pressure at recess 5 exceeds the supply pressure indicating that there is backflow through the orifice. These results are to be taken with caution, since the analysis presumes the flow-orifice relation to be valid for any flow direction. However, experimental evidence presented by Redecliff and Vohr (1969) shows that, for high eccentricity operation, recess pressures larger than the external supply pressure are indeed possible.

Figure 5 shows the predicted film forces, $-F_x$ and F_y, parallel and normal to the static journal displacement, respectively. For the journal speed considered, 500 Hz(30000 rpm), the hydrodynamic effects are dominant and determine a normal force F_y larger than the hydrostatic force F_x. The angle between the resultant load and the eccentricity vector is equal to 56^o and remains relatively constant for the entire range of eccentricity radii considered. For small to moderate eccentricities, the film forces are linear with the static displacement and will determine constant stiffness coefficients. For large static displacements toward the middle of a recess, the curvature of the film forces is upward due to fluid cavitation. However, for displacements toward the mid-land, the film forces curvature is first inward reducing the film forces and then, outwards increasing the forces. This seemingly strange effect is explained in terms of the pressure field not being able to develop substantially in the convergent portion of the film thickness due to the presence of recess 5, and thus pushing water back-flow through the orifice.

Figures 6 through 8 show the calculated synchronous stiffness, damping, and inertia coefficients for the hydrostatic bearing operating at 30000 rpm. The rotordynamic coefficients are uniform for small to moderate journal eccentricity radii. The cross-coupled stiffness coefficients shown in Figure 6 are substantially larger than the direct coefficients and demonstrate the dominance of hydrodynamic effects on the bearing dynamic performance. For large static journal displacements, the bearing direct stiffness (K_{xx}) increases dramatically due mainly to the effect of fluid film cavitation. Figures 7 and 8 show the

direct damping and inertia coefficients to be one order of magnitude larger than the cross coupled damping and inertia coefficients. The magnitude of the direct inertia coefficients is large due to the large density of the fluid and the low clearance to bearing radius ratio. At the concentric position, the direct inertia coefficient is equal to 17.9 Kg and determines for synchronous excitation at 500 Hz(30000 rpm) a reduction of almost 88.3% in the dynamic stiffness ($K_{xx}-\omega^2 M_{xx}$). This result proves that fluid inertia is of utmost importance in the dynamic performance of hydrostatic bearings handling fluids of large density.

The calculated rotordynamic coefficients for an excitation frequency equal to the rotating speed are not affected by the compressibility of the fluid at the recess volume due to the low recess depth to clearance ratio of the designed test bearing. However, for supersynchronous excitations well above the rated journal rotational speed, compressibility effects become important and may cause significant losses in damping and increased values of direct stiffness.

The results obtained for the test bearing dynamic coefficients prompted the question of the test rotor-bearing stability characteristics. Appendix A presents the criteria derived for the threshold speed of instability and whirl frequency ratio of a simple flexible rotor supported on identical bearings and includes the effect of the inertia force coefficients. This effect is significant in the present application.

Figure 9 presents the calculated whirl frequency ratio (ϕ) versus the journal eccentricity for the rotor-bearing system studied. The calculated results show that the whirl ratio is independent of the rotor flexibility and equal to 0.492 for small to moderate static journal center displacements. For the largest positive eccentricities (journal displacement towards the middle of a recess), the whirl ratio drops sharply to a value equal to 0.36. However, for large displacements toward the middle of a land (negative eccentricity ε_x) the whirl ratio increases well above 0.5. This abnormal effect is due to the loss in direct stiffness and the inability of the bearing to attain high pressures at the film lands due to orifice backflow. The results presented clearly show that the dynamic characteristics of the test hybrid bearing are no better than for a plain journal bearing.

Figure 10 presents the threshold speed of instability for the test rotor-bearing system. The rotor mass is equal to 30.84 Kg and the shaft is considered as rigid. The figure includes the predicted onset speed Ω_s if fluid inertia effects are neglected. A net reduction in critical speed of almost 25% is observed to occur due to the large influence of the inertia force coefficients on the stability response of the test system.

CONCLUSIONS

The effect of journal eccentricity on the static and dynamic performance of a water lubricated, 5-recess hybrid bearing is presented in detail. The hydrostatic bearing has been designed to operate at a speed of 30Krpm and a large level of external pressurization(6.64MPa). These operating conditions determine the flow in the bearing to be highly turbulent and strongly dominated by fluid inertia effects.

The numerical predictions are based on the full turbulence-inertial analysis of SanAndres(1989a). The analysis covers the spectrum of journal center displacements directed towards the middle of a recess and towards the mid-land portion between 2 consecutive recesses. Bearing flow rate decreases and friction torque increases as the eccentricity increases. Film forces are linear with the eccentricity for small to moderate static journal center displacements. For large eccentricities, film forces are affected by fluid cavitation and present some unusual features. For large static displacements towards the mid-land it is observed that back flow through the orifices occurs. This unexpected behavior degrades considerably the static as well as the dynamic performance of the bearing.

The dynamic force coefficients for the test bearing are predicted to be constant for small to moderate values of the journal eccentricity. However, for large static displacements toward the mid-land it is observed that the direct force coefficients are substantially reduced. Direct inertia force coefficients of substantial magnitude are predicted in the present application. The levels obtained are a direct consequence of the large density of the fluid considered.

Hydrostatic bearings operating in hybrid mode at high rotational speeds present similar stability characteristics as plain journal bearings. For a single mass flexible rotor supported on HJBs, the threshold speed of instability is reduced by the rotor flexibility and the fluid inertia effect. The cross-coupled inertia coefficients are shown to degrade the stability response of the bearing by reducing the whirl frequency ratio.

APPENDIX A
Linear Stability Analysis

Criteria for the threshold speed of instability and whirl frequency ratio of simple rotor-bearing systems are well known in the literature (Lund, 1965, Chen et al., 1985). These analyses usually consider a rigid or flexible, single mass rotor supported in bearings which possess stiffness and damping characteristics. The influence of inertia force coefficients in the stability of these rotor-bearing systems has not been accounted due presumably to the general assumption that these coefficients are negligible in most circumstances. However, the calculated inertia force coefficients for the present application are rather large compared to the mass of the test rotor, and thus, their effect on the stability of the system is regarded as important.

Consider a single rotor of mass $2M_r$ supported on a pair of identical bearings by a massless shaft of stiffness $2K_r$. Instability sets in at a rotational speed Ω_s when the journal starts a forward precessional motion at the whirl frequency $\omega_s = \phi\ \Omega_s$. From the solution of the homogeneous system of equations for the motion of the rotor and bearing supports, it is determined that the whirl speed ω_s and the whirl frequency ratio ϕ are easily obtained from the following quartic equations:

$$\frac{M_r}{K_r}\,\alpha_i\,\omega_s^4 - \left[\,1+\alpha_i + \frac{K_{eq}}{K_r}\,\right]\omega_s^2 + \frac{K_{eq}}{M_r} = 0 \qquad (A.1)$$

and

$$\phi^4\, I_4 + \phi^2\,(\,I_2 - 1) + \phi_o^2 = 0 \qquad (A.2)$$

where

$$\alpha_i = \frac{(M_{xx}+M_{yy})-2I_1}{2M_r}$$

$$K_{eq} = \frac{K_{xx}C_{yy}+C_{xx}K_{yy}-C_{yx}K_{xy}-C_{xy}K_{yx}}{Cxx+Cyy}$$

$$I_1 = \frac{C_{yx}M_{xy}+C_{xy}M_{yx}}{C_{xx}+C_{yy}} \qquad (A.3)$$

$$I_2 = \frac{K_{xy}M_{yx}+K_{yx}M_{xy}-I_1(K_{xx}+K_{yy})+2K_{eq}I_1}{C_{xx}C_{yy}-C_{xy}C_{yx}}$$

$$I_4 = \Omega_s^2\,\frac{I_1^2-M_{xy}M_{yx}}{C_{xx}C_{yy}-C_{xy}C_{yx}}$$

and

$$\phi_o^2 = \frac{(K_{eq}-K_{xx})(K_{eq}-K_{yy})-K_{xy}K_{yx}}{\Omega_s^2\,(C_{xx}C_{yy}-C_{xy}C_{yx})} \qquad (A.4)$$

If fluid inertia effects are eliminated, then the coefficients α_i, I_1, I_2 and I_4 are equal to zero, and the stability formulae derived are identical to the criteria presented by Lund (1965) and Chen(1985). From equation (A.1) it is determined that the fundamental effect of fluid inertia is to reduce the threshold speed of instability if the ratio of masses α_i is large.

For operation at the concentric position ($\varepsilon_x=\varepsilon_y=0$), the direct dynamic coefficients are identical and the cross-coupled coefficients differ in sign. At this condition, the whirl frequency ratio is obtained from the expression:

$$\phi^2\,\Omega_s^2\,M_{xy} + \phi\,\Omega_s\,C_{xx} - K_{xy} = 0 \qquad (A.5)$$

where it is noted that the whirl ratio is reduced if the cross-coupled inertia coefficient Mxy is negative.

REFERENCES

Artiles, A., Walowit J., and W. Shapiro, 1982, "Analysis of Hybrid Fluid Film Journal Bearings with Turbulence and Inertial Effects," Advances in Computer Aided Bearing Design, ASME Publication G00220, pp. 25-52.

Chaomleffel J.P. and D. Nicholas, 1986, "Experimental Investigation of Hybrid Journal Bearings," Tribology International, Vol. 19, No 5, pp.253-259.

Chen, Y.S., H.Y. Wu, and P.L. Xie, 1985, "Stability of Multirecess Hybrid Operating Oil Journal Bearings," ASME Journal of Tribology, Vol. 107, pp. 116-121.

Constantinescu, V.N. and S. Galetuse, 1975, "Pressure Drop Due to Inertia Forces in Step Bearings," ASME Paper 75-Lub-34.

Deguerce B., and D. Nicholas, 1975, "Turbulent Externally Pressurized Bearings - Analytical and Experimental Results," Conference on Hybrid Bearings, Proc. Instn. Mech. Engnrs., paper XII(ii), pp. 228-233.

Heller, S., 1974,"Static and Dynamic Performance of Externally Pressurized Fluid Film Bearings in the Turbulent Regime," ASME Journal of Lubrication Technology, pp. 381-389.

Hirs G.G., 1973, "A Bulk Flow Theory for Turbulence in Lubricant Films," ASME Journal of Lubrication Technology, pp. 173-146.

Lund, J.W., 1965, "The Stability of an Elastic Rotor in Journal Bearings with Flexible, Damped Supports," ASME Journal of Applied Mechanics, pp. 911-920.

Nelson C.C., and D.T. Nguyen, 1987, "Comparison of Hir's equation with Moody's equation for Determining Rotordynamic Coefficients of Annular Pressure Seals," ASME Journal of Lubrication Technology, Vol. 109, pp. 144-148.

Redecliff, J.M. and J.H. Vohr, 1969, "Hydrostatic Bearings for Cryogenic Rocket Engine Pumps," ASME Journal of Lubrication Technology, pp. 557-575.

San Andres, L., 1989a, "Turbulent Hybrid Bearings with Fluid Inertia Effects, Part 1: Analysis," submitted for review to ASME Journal of Tribology.

San Andres, L., 1989b, "Turbulent Hybrid Bearings with Fluid Inertia Effects, Part 2: Results," submitted for review to ASME Journal of Tribology.

Van Doormaal J.P., and G.D. Raithby, 1984, "Enhancements of the SIMPLE Method for predicting Incompressible Fluid Flows," Numerical Heat Transfer, Vol. 7, pp. 147-163.

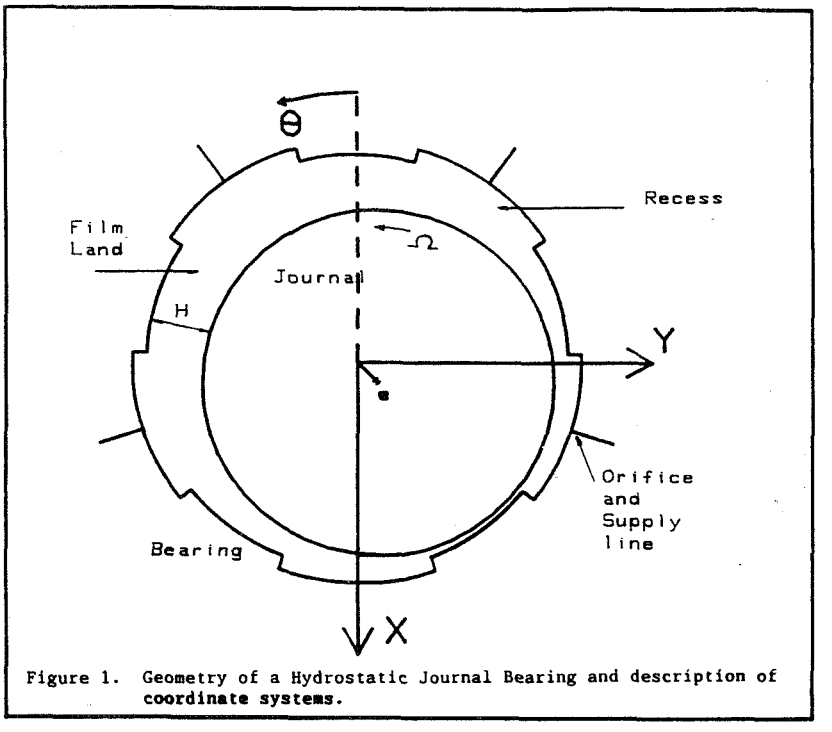

Figure 1. Geometry of a Hydrostatic Journal Bearing and description of coordinate systems.

5 Recess Hydrostatic Water Bearing
TAMU Experimental Program (1989)

Geometry:
Diameter = 76.2mm(3.00 in)
Length = 76.2mm(3.00 in)
Recess lxb = 27mm x 27mm

Clearance = 0.0762mm(0.003in)

Recess depth Hr = 0.457mm(0.018in)

Orifice diameter = 1.496mm

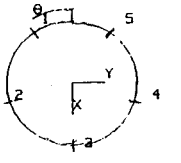

Fluid: Water at 71.1C(160F)
Viscosity, 3.98E-4 Pa sec
Density: 977 Kg/m3

Pressure Supply:6.54MPa(950psi)

Journal speed: 0 to 30000 rpm

Dimensionless Parameters

Reynolds Numbers: Rep=467000,Re*=935.0
Speed ParameterΛ: 0 to 0.04783
Rotation Reynolds Number: 0 to 22360

L/D=1, l/L=.354, N·b/πD=.113
c/R=0.002, Hr/c=6

Table 1. Description of 5 recess hydrostatic water bearing under development for TAMU Hybrid Bearing Research program (1989) Bearing geometry and operating conditions.

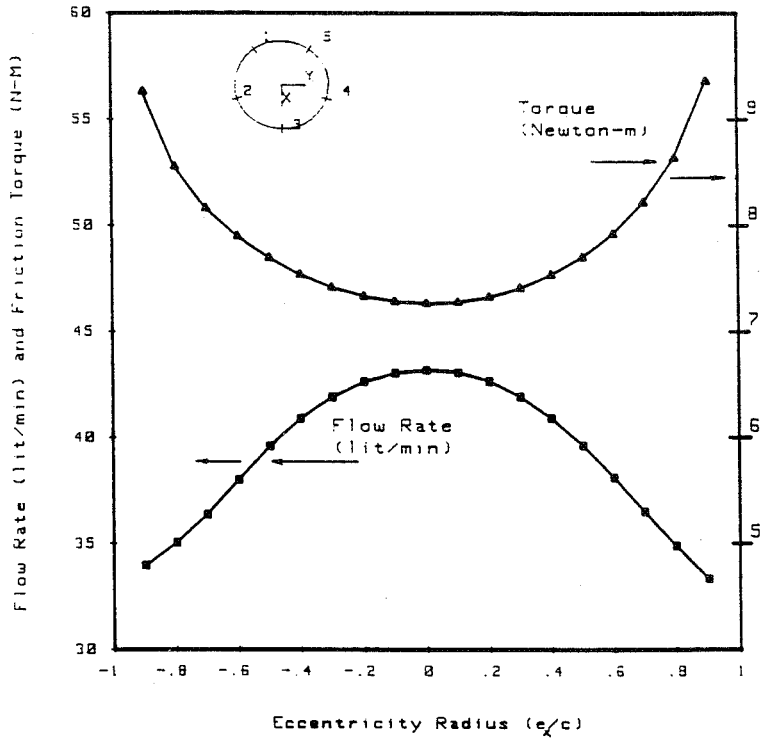

Figure 2. Predicted flow rate and friction torque for test hydrostatic water bearing as a function of static journal eccentricity. Pressure supply equal to 6.54MPa(950psi) and journal speed equal to 500Hz(30000 rpm). Orifice diameter equal to 1.496 mm.

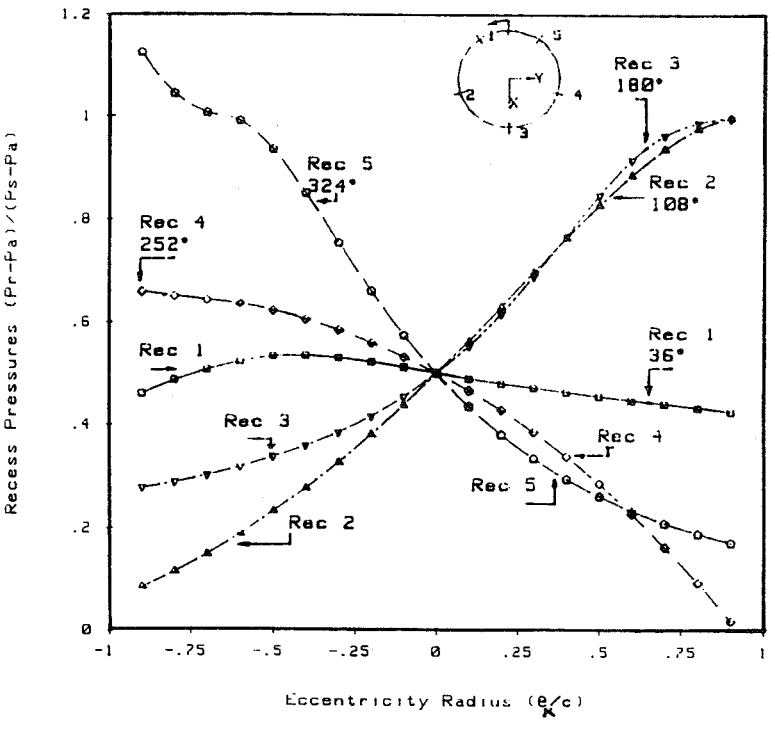

Figure 3. Predicted dimensionless recess pressure for test hydrostatic water bearing as a function of static journal eccentricity. Pressure supply equal to 6.54MPa(950psi) and journal speed equal to 500Hz(30000 rpm). Orifice diameter equal to 1.496 mm.

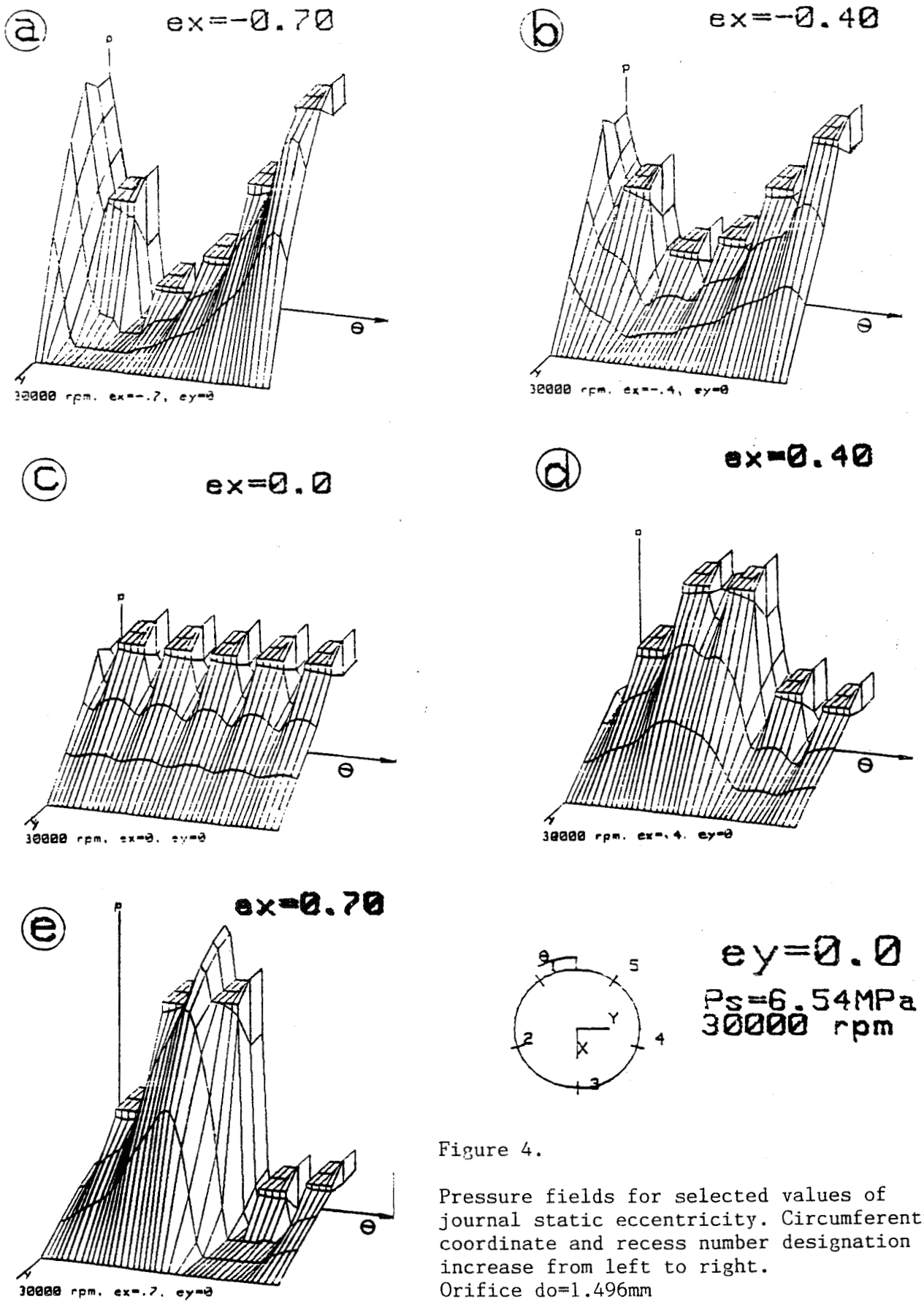

Figure 4.

Pressure fields for selected values of journal static eccentricity. Circumferential coordinate and recess number designation increase from left to right.
Orifice do=1.496mm

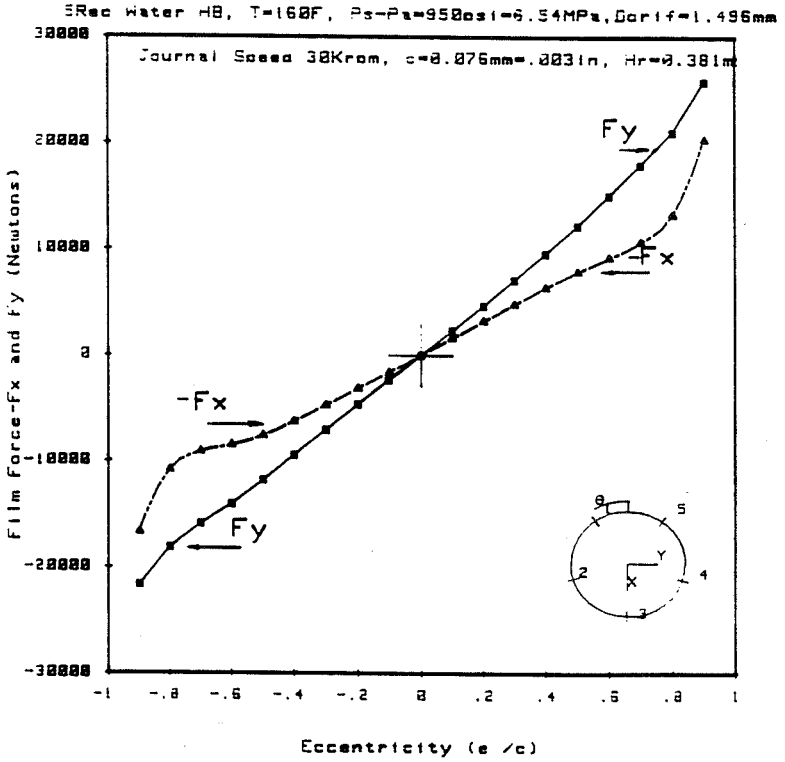

Figure 5. Film forces parallel($-F_x$) and normal(F_y) to journal static displacements for test hydrostatic water bearing. Ps=6.54 MPa, 30000 rpm, orifice diameter=1.496 mm.

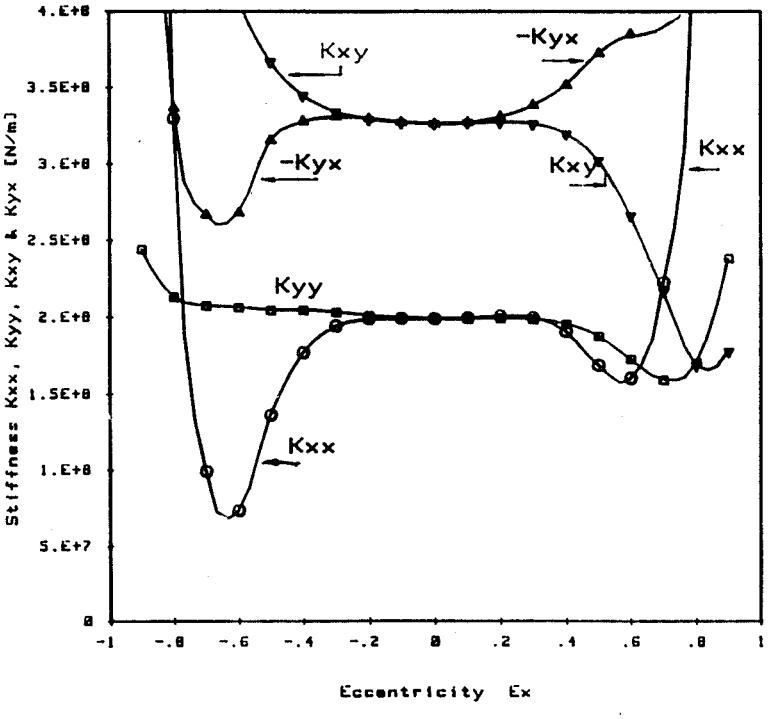

Figure 6. Predicted stiffness coefficients for test hydrostatic water bearing versus journal static eccentricity. Ps=6.54 MPa, 30000 rpm, orifice diameter=1.496 mm.

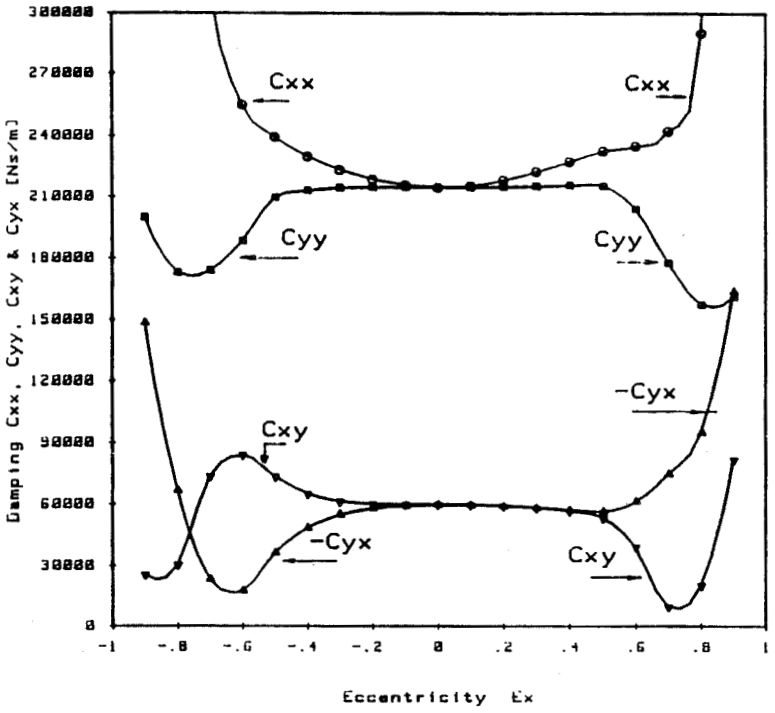

Figure 7. Predicted damping coefficients for test hydrostatic water bearing versus journal static eccentricity. Ps=6.54 MPa, 30000 rpm, orifice diameter=1.496 mm.

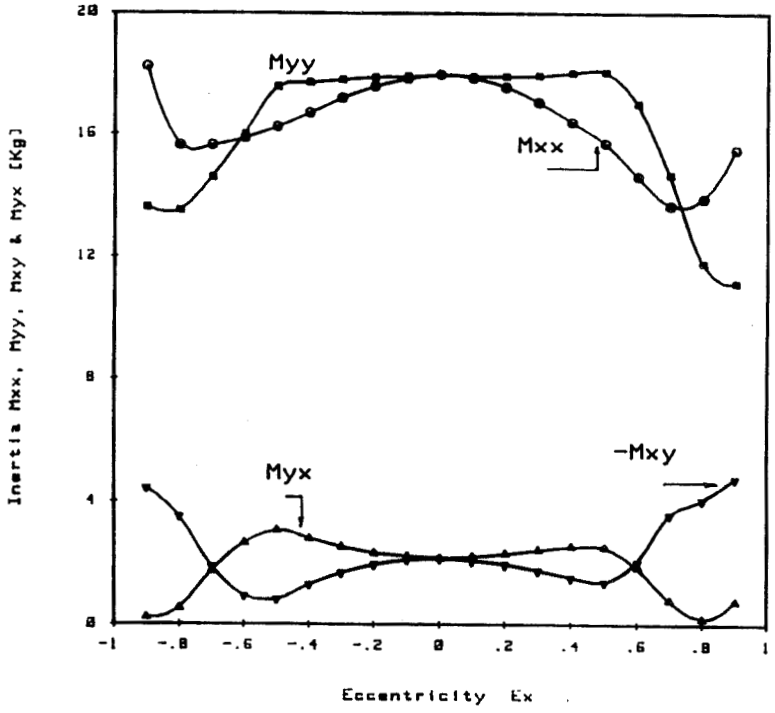

Figure 8. Predicted inertia force coefficients for test hydrostatic water bearing versus journal static eccentricity. Ps=6.54 MPa, 30000 rpm, orifice diameter=1.496 mm.

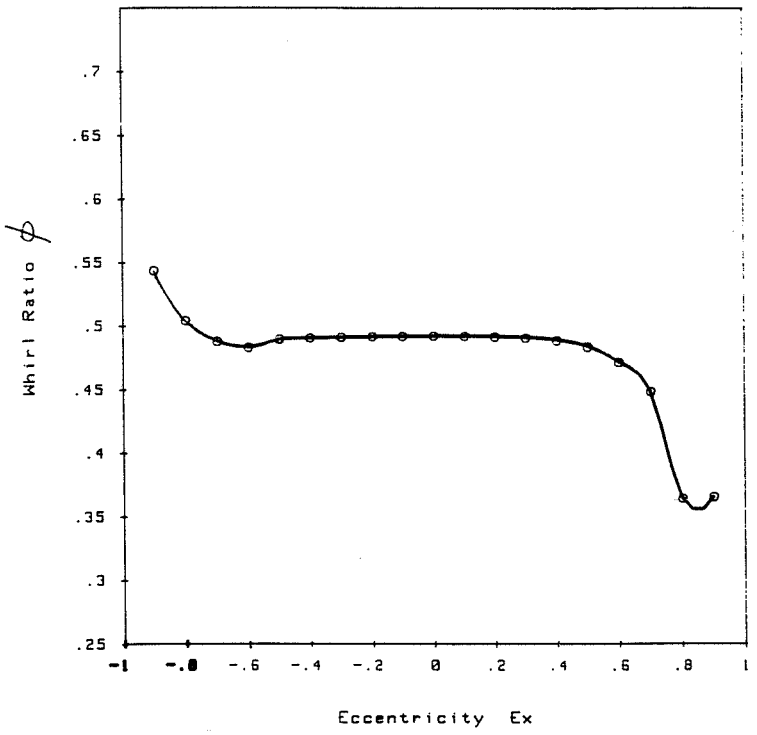

Figure 9. Whirl frequency ratio ϕ for test rotor-hybrid bearing system versus journal static eccentricity.

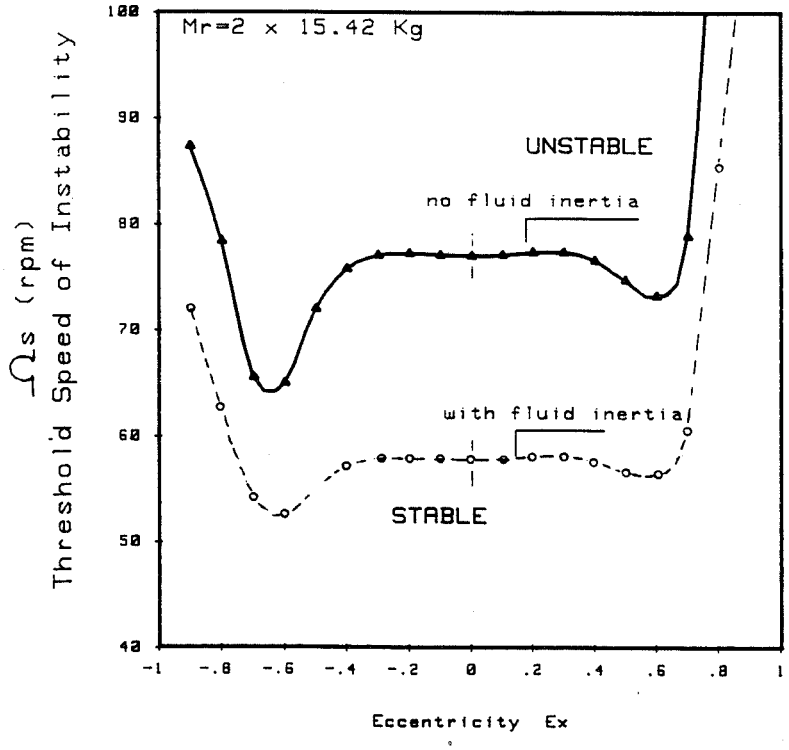

Figure 10. Threshold speed of instability Ω_s for test rotor-hybrid bearing system versus journal static eccentricity.